Electronic Supplementary Material (ESI) for Journal of Materials Chemistry C.
This journal is © The Royal Society of Chemistry 2023

Supporting Information

A New Eco-friendly and Highly Emitting Mn-based Hybrid Perovskite Toward High-Performance Green Down-Converted LEDs

Asmae Ben Abdelhadi,[1,2] Mario Gutiérrez,[1] Boiko Cohen,[1] Luis Lezama,[3] Mohammed Lachkar [2] and Abderrazzak Douhal[*1]

[1]Departamento de Química Física, Facultad de Ciencias Ambientales y Bioquímica, e INAMOL, Campus Tecnológico de Toledo, Universidad de Castilla-La Mancha (UCLM), Avenida Carlos III, S.N., 45071 Toledo, Spain.

[2]Engineering Laboratory of Organometallic, Molecular Materials, and Environment (LIMOME), Faculty of Sciences, Sidi Mohamed Ben Abdellah University, 30000 Fez, Morocco.

[3]Departamento de Química Orgánica e Inorgánica, Facultad de Ciencia y Tecnología, Universidad del País Vasco, UPV/EHU, Bº Sarriena s/n, 48940 Leioa, Spain.

[*]Correspondence: abderrazzak.douhal@uclm.es

Index

1.1. Materials

Tri-n-propylamine ($(C_3H_7)_3N$), 99% aq. soln.) was purchased from Merck. Manganese (II) bromide tetrahydrate ($MnBr_2.4H_2O$, 98%) was obtained from Acros Organics (Spain). Hydrobromic acid (HBr, 48% w/w aq. soln.) and Anhydrous methanol (99.7%) were obtained from Alfa Aesar (Spain).

All chemicals were of reagent grade and were used without further purification. All manipulations were conducted in the air.

1.2 Synthesis of tri-n-propylammonium bromide salt (TPA-Br)

The tri-n-propylammonium bromide salt was prepared by a direct reaction between tri-n-propylammonium (TPA) and Hydrobromic acid (HBr) using ethyl acetate as solvent under continuous stirring at (0-2 °C) in an ice bath to remove the reaction heat. The colorless precipitate was washed several times using ethyl acetate to obtain a clean product. The solvent was evaporated under reduced pressure using a rotary evaporator at 50 °C.

1.3 Synthesis of $(TPA)_2MnBr_4$ single crystals

The synthesis of the $(TPA)_2MnBr_4$ compound was carried out using a similar procedure reported elsewhere.[1] After dissolving 0.44 g (2 mmol) of tri-n-propylammonium bromide (TPA-Br) and 0.286 g (1 mmol) of manganese (II) bromide tetrahydrate ($MnBr_2.4H_2O$) in water, 3 mL of 80 % HBr were added to the solution, and the mixture was stirred for 2 h until the solid was completely dissolved. The corresponding chemical reaction is presented in (Eq. 1):

$$2\left[(C_3H_7)_3N^+, Br^-\right] + MnBr_2.4H_2O \rightarrow \left[(C_3H_7)_3N\right]_2MnBr_4 \quad (1)$$

The solution was then evaporated to almost dryness at 45 °C. After 3 days, light pink needle single crystals of $(TPA)_2MnBr_4$ were obtained.

1.4 Synthesis of $(TPA)_2MnBr_4$ powder

0.224 g (1 mmol) of tri-n-propylammonium bromide and 0.286 g (1 mmol) of manganese (II) bromide tetrahydrate were mixed in 4mL of anhydrous methanol solvent for 2h at room temperature. Later, the solution was kept at 40 °C for several days until the solvent was completely evaporated and a light-yellow powder of $(TPA)_2MnBr_4$ was obtained.

The fresh products showed a bright green fluorescence under UV light irradiation. The prepared powder was kept in a desiccator to prevent its exposition to moisture.

1.5 Fabrication of green-light-emitting diodes LEDs

The down-converter LED devices were fabricated by combining a 465 nm UV LED chip with the as-synthesized green-phosphor $(TPA)_2MnBr_4$. The color of the LEDs was tuned by controlling the amount of the green-phosphor $(TPA)_2MnBr_4$, which is varied from 4-10mg. The LEDs were operated at 2.7V and a drive current of 18mA.

1.6 Characterizations and measurements

For the single crystal X-ray measurements, a suitable crystal of 0.15×0.12×0.08 mm^3 was selected and placed on a MiTeGen micromount on an XtaLAB Synergy R, HyPix-Arc 100 diffractometer. The crystal was kept at a steady T = 150.00(10) K during data collection. The structure was solved with the SHELXT 2018/2[2] structure solution program using the Intrinsic Phasing solution method and by using Olex2[3] as the graphical interface. The model was refined with version 2018/3 of SHELXT 2018/344 using Least Squares minimization. All non-hydrogen atoms were refined anisotropically. Hydrogen atom positions were calculated geometrically and refined using the riding model. Important structural refinement parameters are summarized in Tables S1-S3 and the crystallographic data are also supplied. The DIAMOND program was used for the crystal structure plotting.[4] The crystallographic data are deposited in the Cambridge Crystallographic Data Centre (CCDC 2301462). The data can be downloaded from the site (www.ccdc.cam.ac.uk/data_request/cif).

The Hirshfeld surfaces and the 2D finger plots of $(TPA)_2MnBr_4$ were generated by the program Crystal Explorer 3.1[5] based on the CIF files. To identify the regions of particular importance to the intermolecular interactions (highlighted by red, white and blue areas), the normalized contact distance (d_{norm}) was generated using the following equation (2):

$$d_{norm} = \frac{(d_i - r_i^{vdw})}{r_i^{vdw}} + \frac{(d_e - r_e^{vdw})}{r_e^{vdw}} \quad (2)$$

based on d_e (distance from the surface to the nearest atom exterior to the surface), d_i (distance from the surface to the nearest atom interior to the surface) and r^{vdw} the van der Waals radii of the atom.

The powder X-ray diffraction (PXRD) of the powder particles of the synthesized perovskites obtained from the grounded single crystals previously used for the crystal structure determination was carried out using a PANalytical diffractometer (X'Pert Pro model) and an X Bruker D8 Advance. The conditions used were 45 kV, 40 mA, CuKα radiation, and a system of slits (soller-mask-divergence-antiscatter) of 0.04 rad-10 mm-1/8◦ -1/4◦ with an X'celerator detector.

Thermogravimetric analysis (TGA) and differential scanning calorimetry (DSC) analysis of synthesized compound (DSC) were undertaken on a SDT Q600 calorimeter under the dynamic Nitrogen (100 mL/min flow rate) in temperature range of 25–900 °C at the scan rate of 10 °C/min. The sample weight was 10.36 mg. Platinum crucibles were used as containers.

X-band (~9.36 GHz) EPR measurements were carried out on a Bruker ELEXSYS 500 spectrometer equipped with a super-high-Q resonator ER-4123-SHQ and standard Oxford Instruments low-temperature devices. Q-band (~33.9 GHz) EPR spectra were recorded on a Bruker EMX system equipped with an ER-510-QT resonator. The magnetic field was calibrated by a NMR probe and the frequency inside the cavity was determined with a Hewlett-Packard 5352B microwave frequency counter. Data were collected and processed using the Bruker Xepr suite.

The UV/Vis diffuse reflectance (DR) spectra were recorded on a JASCO V-670 spectrophotometer equipped with a 60 mm integrating sphere unit (JASCOISN-723). The longitudinal axes of the spectrum were converted using the Kubelka–Munk function from reflectance (%R) to K-M unit $F(R) = ((1 - R)^2(2R)^{-1})$ where R is the diffuse reflectance intensity from the sample. The emission and excitation spectra were measured by a FluoroMax-4 (Jobin-Yvon) spectrofluorometer. Photoluminescence quantum yield (PLQY) measurements were performed using the quanta-ϕ (HORIBA) integrating sphere accessory, attached to the "NanoLog" Horiba Jobin Yvon spectrofluorometer.

Time-resolved photoluminescence (TR-PL) measurements were performed by exciting the samples with 40 ps-pulsed (<1 mW, 40 MHz repetition rate) diode lasers (PicoQuant, Germany) centered at 371 and 433 nm. The system was equipped with a laser driver (PDL820B, PicoQuant, Germany) for burst operation that allows the measurement of luminescence decays at time windows up to several seconds. The emission decays were collected and analyzed through a TCSPC and multi-channel scaling board (TimeHarp260

(nano), PicoQuant, Berlin, Germany). The fluorescence signal was gated at a magic angle (54.7°) and monitored at 90° with respect to the excitation beam at discrete emission wavelengths. The experimental decays were accurately analyzed using a single exponential function.

Fluorescence Lifetime Imaging. Fluorescence lifetime images were recorded with a MicroTime 200 microscope (PicoQuant) equipped with a TCSPC card and two TAU-SPAD avalanche photodiode detectors. A 390-nm pulsed diode laser (PicoQuant) was used as the excitation source at a 10 MHz repetition rate and a power of ~0.7 μW. FLIM images were processed using SymPhoTime 64 software (PicoQuant). The anisotropy distribution histograms were obtained from the FLIM images collected at parallel an perpendicular orientation of the emission with respect to the excitation. The emission spectra were collected through a Shamrock ST-303i (Andor Technology) imaging spectrograph and detected by an Andor Newton EMCCD camera (Andor Technology).

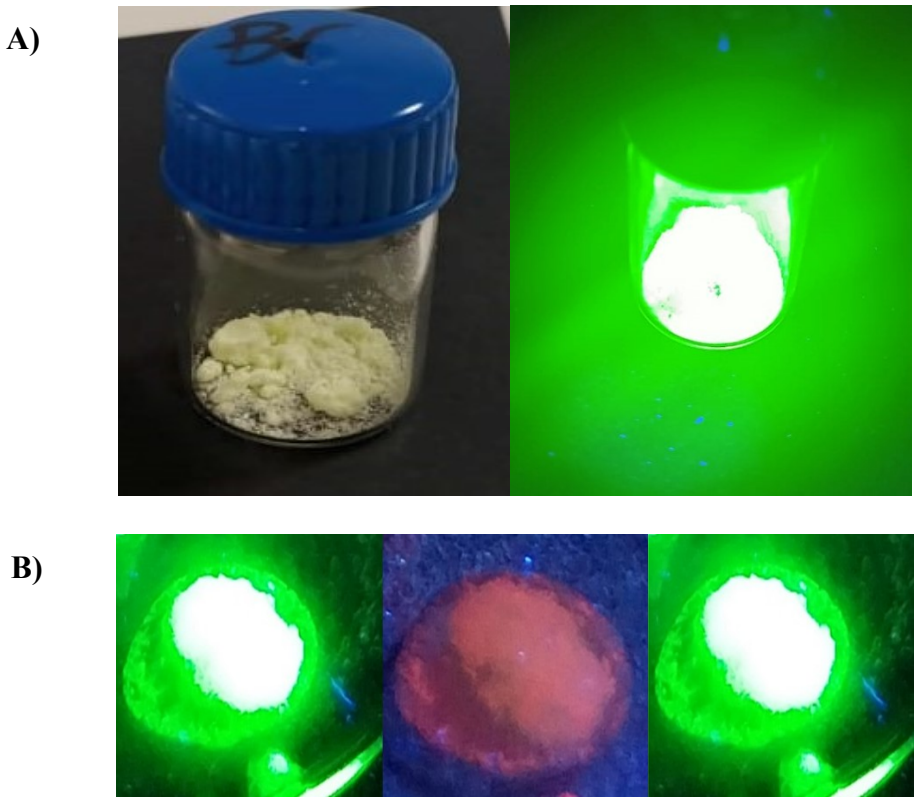

Figure S1. (A) Optical photographs of as-prepared $(TPA)_2MnBr_4$ crystals in the daylight (left) and upon 365 nm UV excitation (right). (B) Representation of the temperature effect on the emission of $(TPA)_2MnBr_4$ upon 365 nm excitation. Left: room temperature before heating; Centre: After heating for 30 min at 75^{O}C, above the melting point, 72^{O}C; Right: After cooling down the melted sample to room temperature.

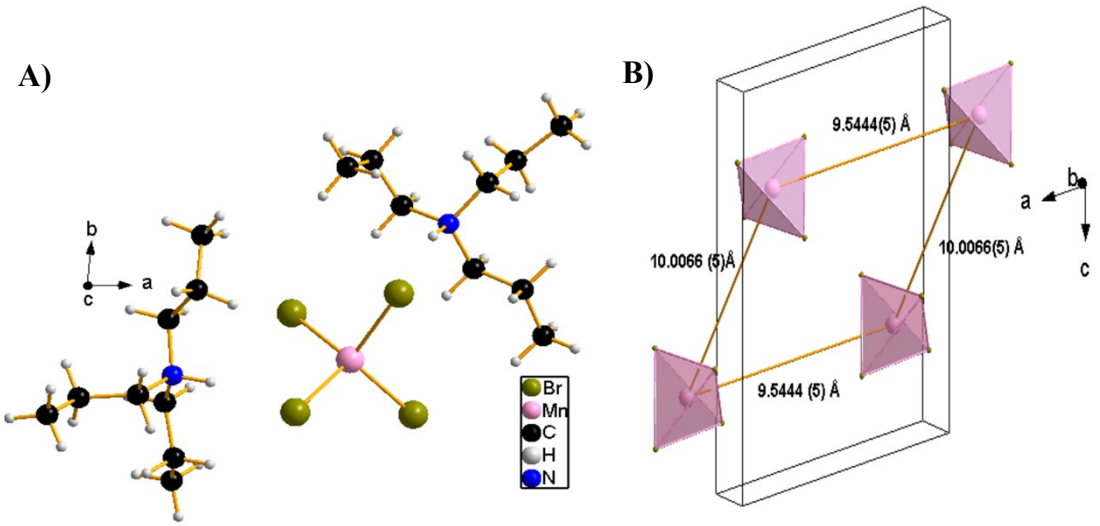

Figure S2. (A) Crystal structure of $(TPA)_2MnBr_4$. (B)The Mn-Mn distances in $(TPA)_2MnBr_4$ are 9.5444 Å and 10.0066 Å labeled with orange lines.

Surface d'Hirchfeld analysis

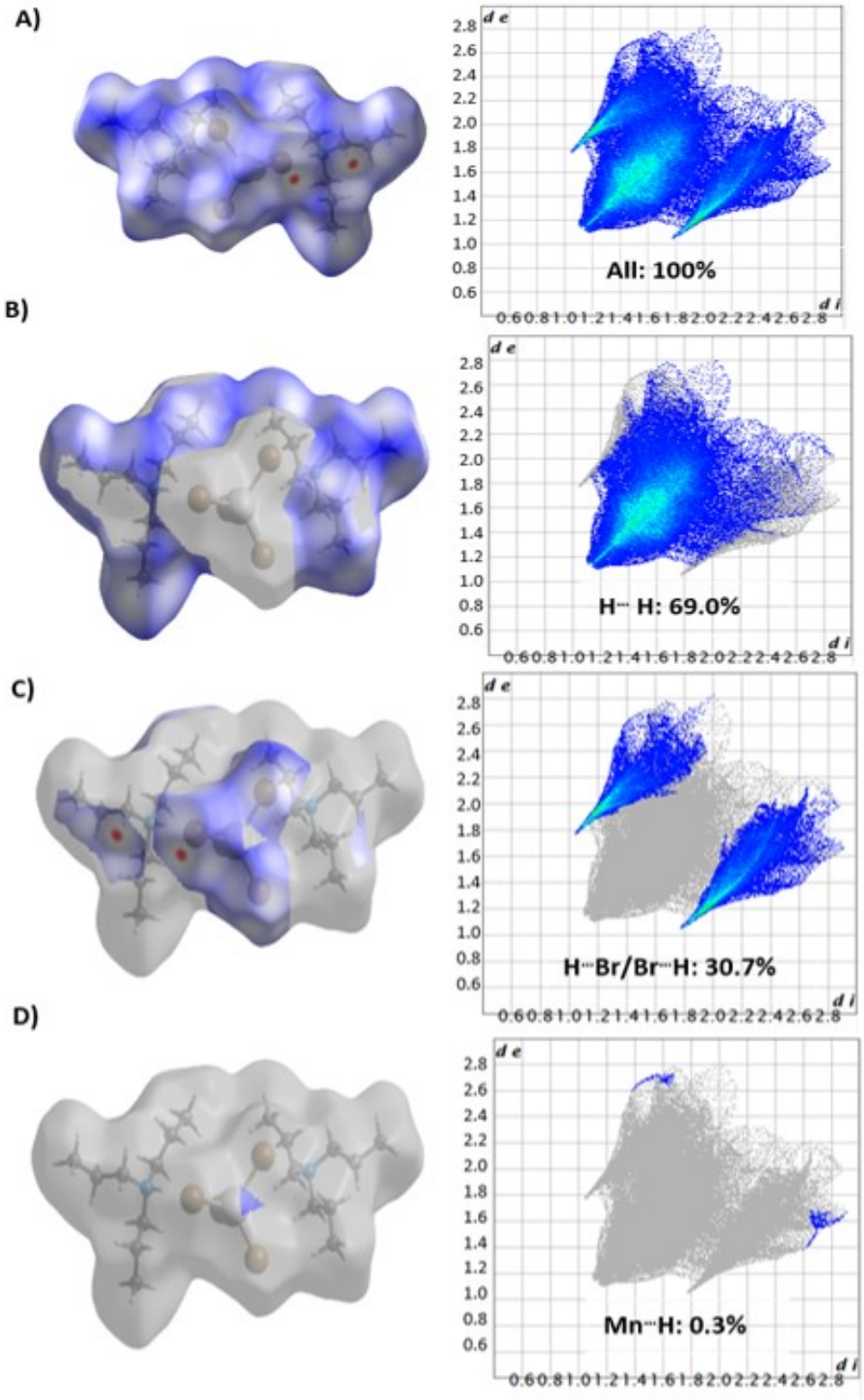

Figure S3. Hirshfeld surface analysis mapped with d_{norm} and the associated 2D-fingerprint plots of $(TPA)_2MnBr_4$ showing the major intermolecular interactions: (A) All, (B) H···H, (C) H···Br/Br···H and (D) Mn···H contributions.

Table S1. Crystallographic Parameters for single crystal of $(TPA)_2MnBr_4$ from Single-crystal X-ray diffraction experiment.

Crystal data	
$Br_4Mn{\cdot}2(C_9H_{22}N)$	$Z = 2$
$M_r = 663.13$	$F(000) = 662$
Triclinic, P_{-1}	$D_x = 1.585$ Mg m^{-3}
$a = 9.5444$ (2) Å, $b = 10.1056$ (2) Å and $c = 15.1835$ (3) Å	Cu $K\alpha$ radiation, $\lambda = 1.54184$ Å
$\alpha = 82.880$ (2)°, $\beta = 73.734$ (2)° and $\gamma = 83.119$ (2)°	Cell parameters from 30197 reflections
$V = 1389.44$ (5) Å^3	$\theta = 3.0–73.1°$
$T = 150$ K	$\mu = 10.62$ mm^{-1}
0.15 × 0.12 × 0.08 mm	Irregular, clear light yellow
Data collection	
XtaLAB Synergy R, HyPix-Arc 100 diffractometer	4923 independent reflections
Radiation source: Rotating-anode X-ray tube, PhotonJet R (Cu) X-ray Source	4731 reflections with $I > 2\sigma(I)$
Mirror monochromator	$R_{int} = 0.025$
Detector resolution: 10.0000 pixels mm^{-1}	$\theta_{max} = 66.6°$, $\theta_{min} = 3.1°$
ω scans	$h = -11 \rightarrow 11$
$T_{min} = 0.206$, $T_{max} = 0.533$	$k = -12 \rightarrow 12$
48346 measured reflections	$l = -18 \rightarrow 18$
Refinement	
Refinement on F^2	Primary atom site location: dual
Least-squares matrix: full	Hydrogen site location: inferred from neighbouring sites
$R[F^2 > 2\sigma(F^2)] = 0.020$	H-atom parameters constrained
$wR(F^2) = 0.045$	$w = 1/[\sigma^2(F_o^2) + (0.0182P)^2 + 1.2243P]$ where $P = (F_o^2 + 2F_c^2)/3$
$S = 0.99$	$(\Delta/\sigma)_{max} = 0.001$
4923 reflections, 232 parameters and 0 restraints.	$\Delta\rho_{max} = 0.53$ e Å^{-3}, $\Delta\rho_{min} = -0.40$ e Å^{-3}

Table S2. Geometric parameters (Å, º) for $(TPA)_2MnBr_4$ single crystal.

Br1—Mn1	2.5076 (4)	C7—N1	1.511 (3)
Br2—Mn1	2.5408 (4)	C8—C9	1.502 (4)
Br3—Mn1	2.5083 (4)	C10—C11	1.499 (4)
Br4—Mn1	2.4896 (4)	C10—N2	1.508 (3)
C1—C2	1.516 (3)	C11—C12	1.519 (4)
C1—N1	1.507 (3)	C13—C14	1.515 (3)
C2—C3	1.520 (3)	C13—N2	1.513 (3)
C4—C5	1.519 (3)	C14—C15	1.518 (4)
C4—N1	1.507 (3)	C16—C17	1.499 (4)
C5—C6	1.524 (3)	C16—N2	1.501 (3)
C7—C8	1.512 (3)	C17—C18	1.516 (4)
Br1—Mn1—Br2	107.948 (15)	C1—N1—C4	113.91 (16)
Br1—Mn1—Br3	111.213 (14)	C1—N1—C7	109.28 (16)
Br3—Mn1—Br2	106.654 (14)	C4—N1—C7	113.61 (17)
Br4—Mn1—Br1	109.779 (15)	C11—C10—N2	113.31 (19)
Br4—Mn1—Br2	111.917 (15)	C10—C11—C12	109.5 (2)
Br4—Mn1—Br3	109.304 (15)	N2—C13—C14	114.37 (19)
N1—C1—C2	114.91 (18)	C13—C14—C15	110.2 (2)
C1—C2—C3	110.49 (19)	C17—C16—N2	113.5 (2)
N1—C4—C5	113.04 (17)	C16—C17—C18	109.9 (2)
C4—C5—C6	110.53 (19)	C10—N2—C13	114.69 (18)
N1—C7—C8	115.6 (2)	C16—N2—C10	110.63 (18)
C9—C8—C7	115.3 (2)	C16—N2—C13	112.90 (18)
C2—C1—N1—C4	49.5 (2)	C11—C10—N2—C13	-57.2 (3)
C2—C1—N1—C7	177.81 (18)	C11—C10—N2—C16	173.7 (2)
C5—C4—N1—C1	61.3 (2)	C14—C13—N2—C10	-51.8 (3)
C5—C4—N1—C7	-64.7 (2)	C14—C13—N2—C16	76.2 (3)
C8—C7—N1—C1	-179.80 (19)	C17—C16—N2—C10	-156.3 (2)
C8—C7—N1—C4	-51.4 (3)	C17—C16—N2—C13	73.7 (2)
N1—C1—C2—C3	177.42 (18)	N2—C10—C11—C12	-173.7 (2)
N1—C4—C5—C6	-170.27 (19)	N2—C13—C14—C15	-176.9 (2)
N1—C7—C8—C9	-60.2 (3)	N2—C16—C17—C18	166.5 (2)

Table S3. Distances (Å) and angles (º) in the hydrogen-bond geometry of $(TPA)_2MnBr_4$ single crystal.

D—H···*A*	*D*—H	H···*A*	*D*···*A*	*D*—H···*A*
C1—H1*A*···Br3^{i}	0.99	2.96	3.904 (2)	160
C5—H5*B*···Br3^{i}	0.99	3.06	3.980 (2)	155
C7—H7*A*···Br3	0.99	3.02	3.982 (2)	166
C7—H7*B*···Br4^{i}	0.99	3.03	3.973 (2)	161
N1—H1···Br2	1.00	2.39	3.3462 (17)	160
C11—H11*B*···Br1	0.99	3.10	3.913 (3)	140
C13—H13*B*···Br1^{ii}	0.99	2.91	3.870 (2)	163
C14—H14*B*···Br2^{iii}	0.99	3.12	4.011 (3)	150
C16—H16*A*···Br3	0.99	2.96	3.724 (2)	135
C16—H16*B*···Br2^{iii}	0.99	3.00	3.875 (2)	148
N2—H2···Br1	1.00	2.36	3.3538 (19)	171

Symmetry codes: (i) -x+2, -y+1, -z; (ii) -x+1, -y, -z+1; (iii) x-1, y, z.

DSC plot

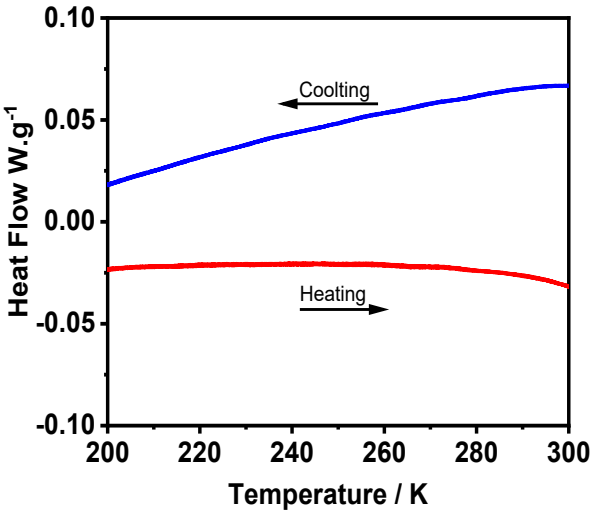

Figure S4. DSC curves during heating and cooling of $(TPA)_2MnBr_4$ measured between 200 and 300 K.

EPR Spectra

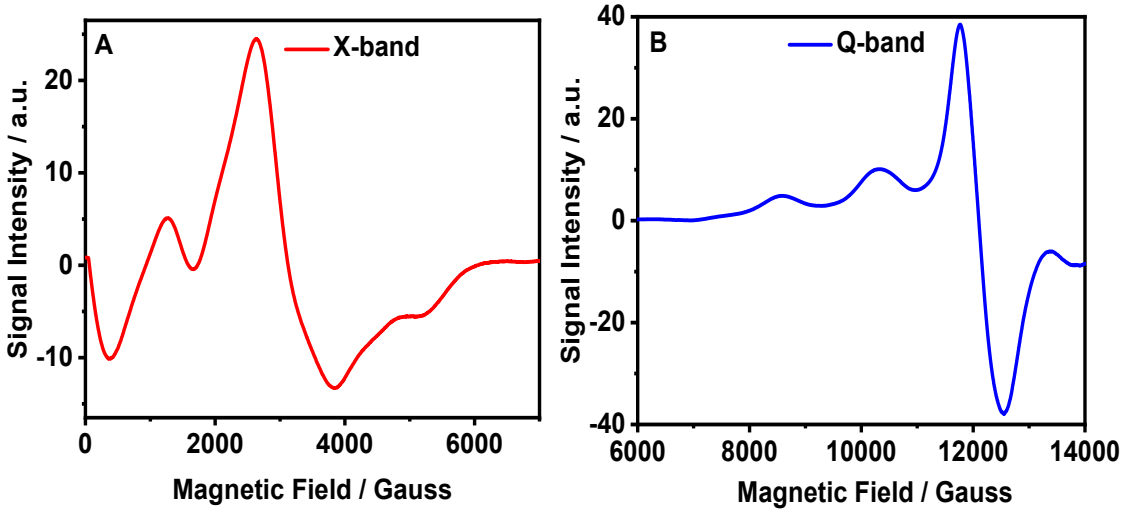

Figure S5. X-band (A) and Q-band (B) electron-spin paramagnetic resonance (EPR) of $(TPA)_2MnBr_4$ at room temperature.

Emission spectra at different excitation wavelengths

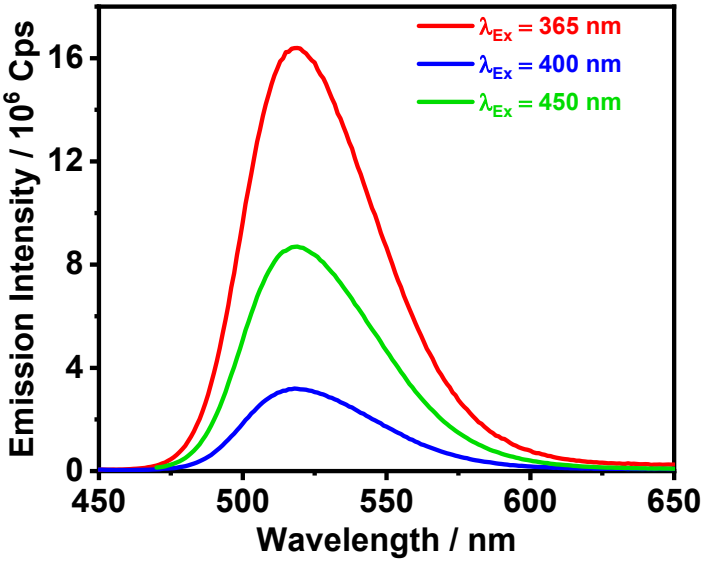

Figure S6. Excitation wavelength-dependent (inset) emission spectra of $(TPA)_2MnBr_4$ at room temperature.

Table S4. Examples of reported single crystals of Mn-based tetrahedral bromide perovskites and their photophysical proprieties.

Examples of reported Mn(II) tetrahedral and Br hybrid perovskites	Mn-Mn distance (Å)	λ_{Em}(nm)	PLQY (%)	Emission Lifetime (ms)	k_{nr} ($10^3 s^{-1}$)	LED	Ref.
$(3AMP)MnBr_4$	6.52	514	9.5	0.025	36.2	No	[6]
Cs_3MnBr_5	6.79	520	49	0.290	1.75862	Yes	[7]
$(EPY)_2MnBr_4$	6.87	515	28.1	0.214	3.35981	Yes	[8]
$(3MP)\ MnBr_4$	7.94	523	13	0.019	45.78947	No	[6]
$(C_{13}H_{26}N)_2MnBr_4$	8.02	515	64.6	0.370	0.95676	Yes	[9]
$(PMMIM)_2MnBr_4$	8.18	515	70.2	0.367	0.81199	Yes	[8]
$(HQ)_2MnBr_4$	8.42	545	38.7	0.335	1.82985	No	[10]
$(IPTMA)_2MnBr_4$	8.52	497	52.6	-	-	No	[11]
$(C_{13}H_{14}N)_2MnBr_4$	8.54	539	46.2	0.245	2.19592	Yes	[9]
$[(CH_2)_4N(CH_2)_4]_2MnBr_4$	8.58	525	13.1	-	-	No	[12]
$(TMPEA)_2MnBr_4$	8.64	520	70.8	0.096	3.04167	No	[6]
$(MeQ)_2MnBr_4$	8.79	528	44.6	0.242	2.28926	No	[10]
$(DIPA)_2MnBr_4$	8.85	525	62.2	$1.4.10^{-6}$	-	No	[13]
$(CH_2CH_3)_3NH)_2MnBr_4$	8.85	528	50	0.380	1.31579	No	[14]
$(EtQ)_2MnBr_4$	8.86	528	64.4	0.349	1.02006	No	[10]
$C_8H_{20}N_2MnBr_4$	8.88	520	19	$3.9.\ 10^{-6}$	-	No	[15]
$(BTMA)_2MnBr_4$	8.97	519	51.1	0.236	2.07203	No	[6]
$(HEP)_2MnBr_4$	9.00	519	25.5	0.049	15.20408	No	[6]
$(C_9H_{14}N)_2MnBr_4$	9.03	521	58	0.335	1.25373	Yes	[8]
$(FEtQ)_2MnBr_4$	9.04	516	83.6	0.370	0.44324	No	[10]
$(EMMIM)_2MnBr_4$	9.09	511	79.5	0.343	0.59767	Yes	[8]
$(BTEA)_2MnBr_4$	9.39	515	46	0.334	1.61677	Yes	[16]
$(C_9NH_{20})_2MnBr_4$	9.41	528	81.1	0.319	0.59248	No	[17]
$(TPA)_2MnBr_4$	9.54	520	62	0.390	0.97436	Yes	This work
$(BTEA)_2MnBr_4$	9.62	521	97.8	0.346	0.06358	No	[18]
$(BMPR)_2MnBr_4$	9.65	527	50.6	0.270	1.82963	Yes	[16]
$(C_{12}H_{28}N)_2MnBr_4$	9.75	511	76	0.329	0.72948	Yes	[8]
$(HTPP)_2MnBr_4$	>10	521	98.6	0.307	0.0456	No	[19]
$(C_8H_{20}N)_2MnBr_4$	10.28	515	85.1	0.443	0.33634	Yes	[20]
$(C_{24}H_{20}P)_2MnBr_4$	10.45	515	99.8	0.372	0.00538	Yes	[21]

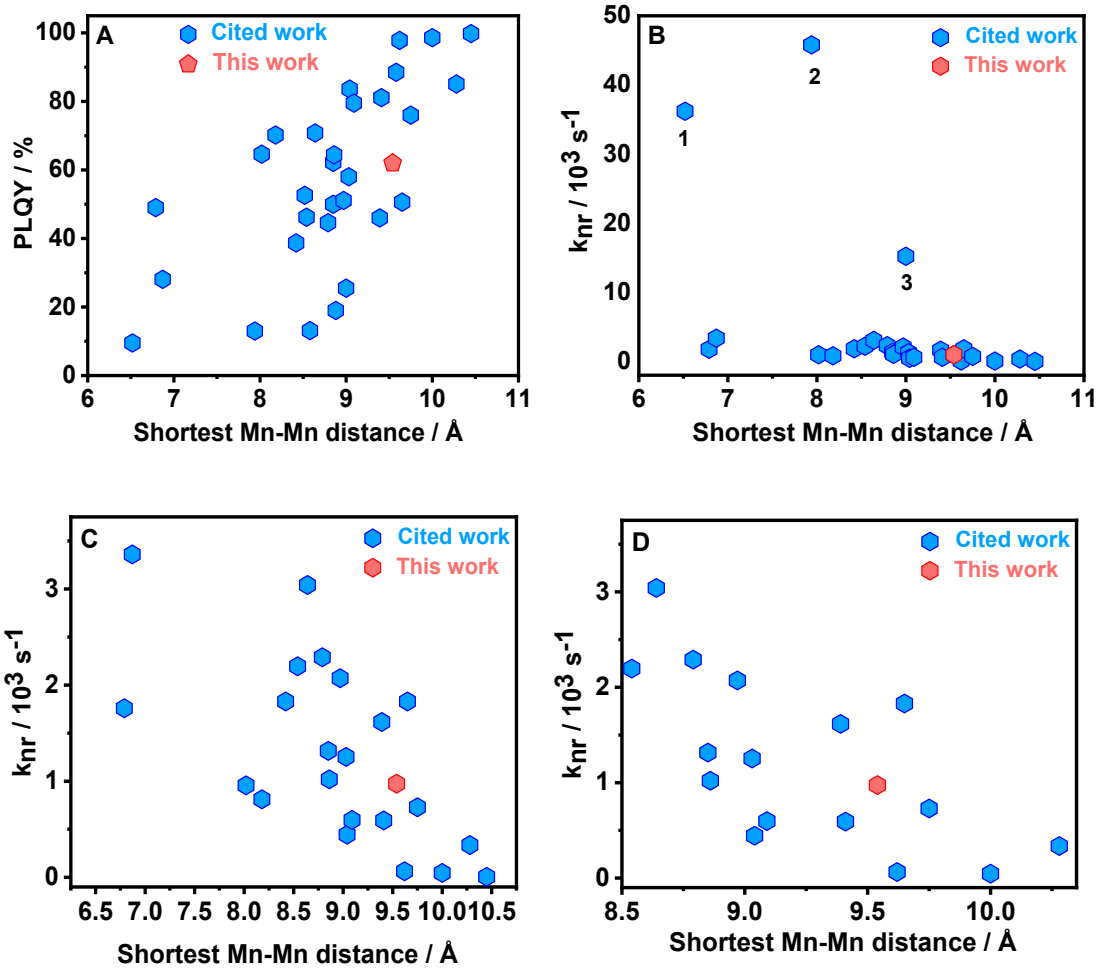

Figure S7. Variation of the Mn-Based tetrahedral hybrid perovskites (A) photoluminescence quantum yield (PLQY) and (B, C and D) non-radiative rate constant (k_{nr}) with the value of the shortest Mn···Mn distance (in single crystal). The plotted data are from table S4. Plot (C) is without the data of perovskites 1-3 in plot (B). Plot (D) is for Mn···Mn distance starting from 8.5 Å. The labeled data, 1, 2 and 3 in panel (B) are for aminomethylpiperidinium (3AMP), 3-methylpiperidinium (3MP) and heptamethylenimine (HEP), respectively.

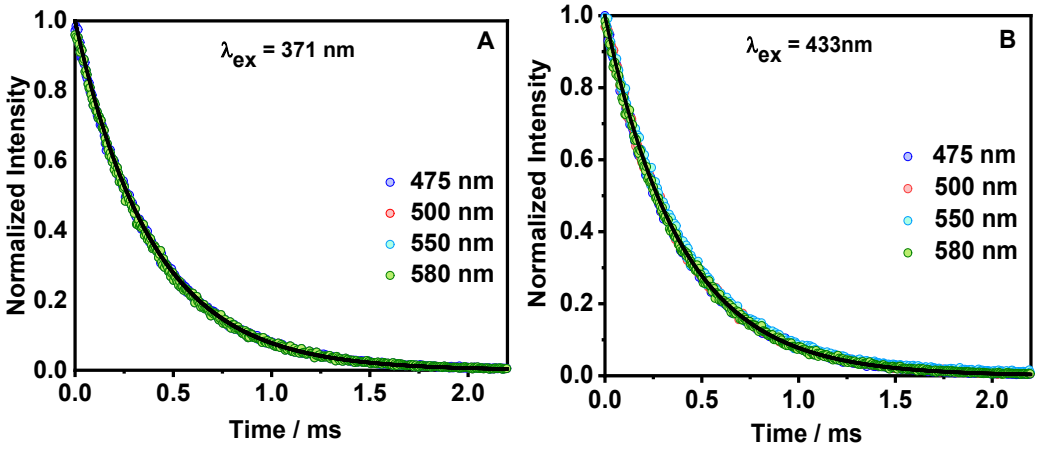

Figure S8. 295 K emission decays of $(TPA)_2MnBr_4$ at the indicated wavelengths of observation under two excitation wavelengths: (A) 371 nm and (B) 433 nm. The solid line is a monoexponetial fit of the experimental decay giving an emission lifetime of 0.390 ms.

Single Crystal Emission Microscopy

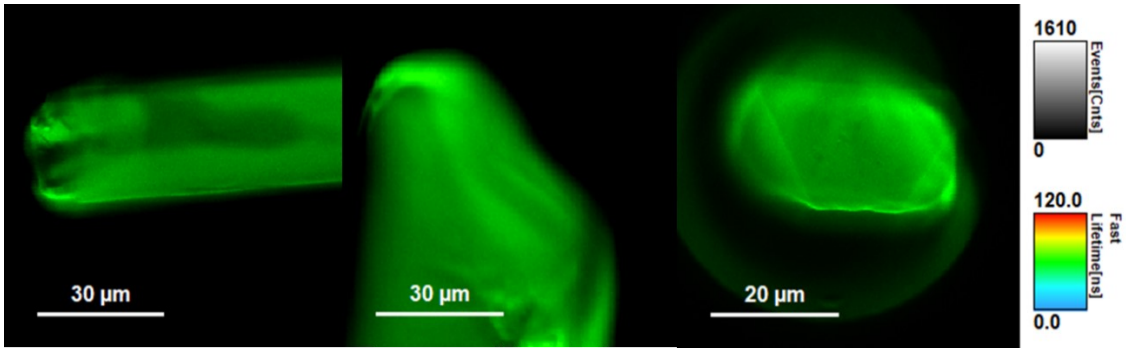

Figure S9. FLIM images of different isolated single crystals of $(TPA)_2MnBr_4$.

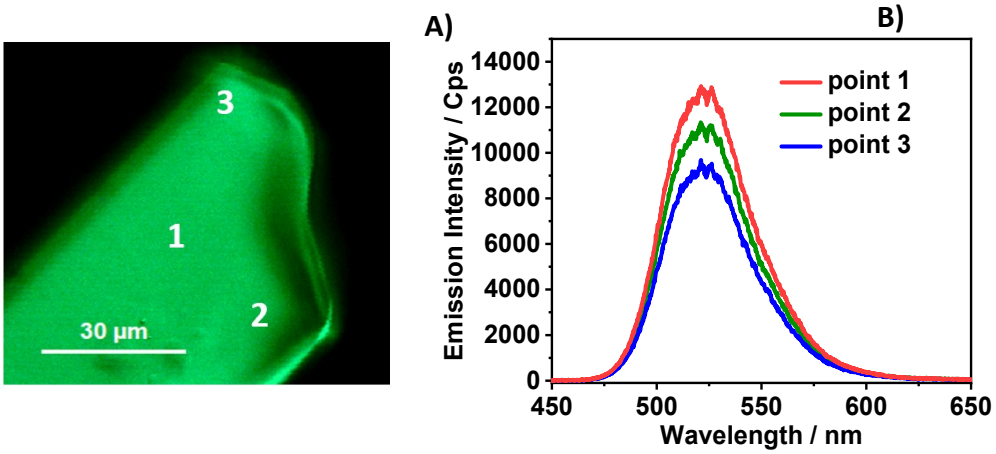

Figure S10. (A) FLIM image of an isolated $(TPA)_2MnBr_4$ crystal and (B) emission spectra collected at discrete points: (1) bulk, (2 and 3) edge.

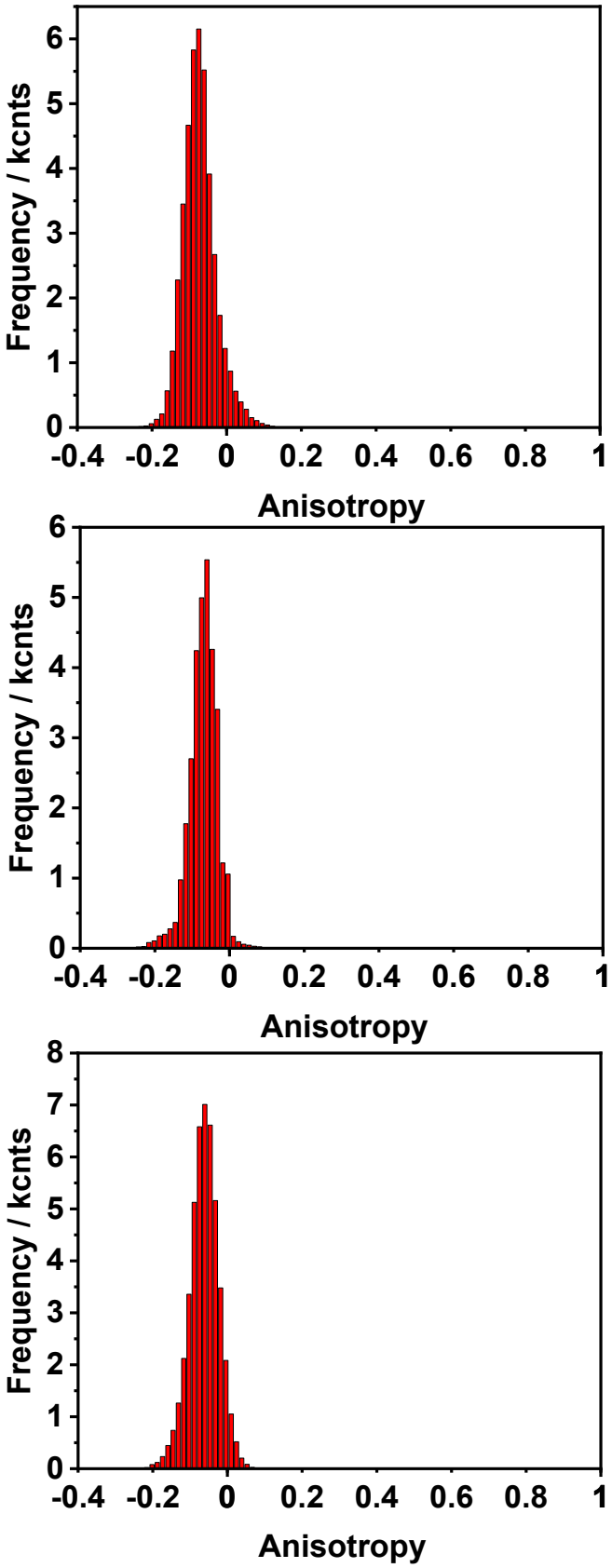

Figure S11. Anisotropy distribution histograms of three different isolated $(TPA)_2MnBr_4$ crystals.

Acknowledgements

This work is supported by the following grants: grant PID2020-116519RB-I00 and TED2021-131650B-I00 funded by MCIN/AEI/10.13039/501100011033 and the European Union (EU); grant SBPLY/19/180501/000212 funded by JCCM and the EU through "Fondo Europeo de Desarollo Regional" (FEDER); grant 2020-GRIN-28929 funded by UCLM (FEDER). A.B.A. thanks the Erasmus+ program of the European Union for financial support. M.G. thanks the EU for financial support through Fondo Social Europeo Plus (FSE+).

References

1. Y. H. Kim and $_{N. Hur}$, *J. Appl. Phys.* , 2021, **129**, 224101.
2. G. M. Sheldrick, *Acta Crystallogr. C Struct. Chem.*, 2015, **71**, 3-8.
3. O. Dolomanov, L. Bourhis, R. Gildea, J. Howard and H. Puschmann, *J. Appl. Cryst.* , 2009, **42**, 339-341.
4. K. Brandenburg and H. Putz, *Crystal Impact GbR, Bonn, Germany*, 2006.
5. S. Wolff, D. Grimwood, J. McKinnon, M. Turner, D. Jayatilaka and M. Spackman, *Journal*, 2012.
6. L. Mao, P. Guo, S. Wang, A. K. Cheetham and R. Seshadri, *J. Am. Chem. Soc.*, 2020, **142**, 13582-13589.
7. B. Su, M. S. Molokeev and Z. Xia, *J. Mater. Chem. C*, 2019, **7**, 11220-11226.
8. Y.-Y. Ma, Y.-R. Song, W.-J. Xu, Q.-Q. Zhong, H.-Q. Fu, X.-L. Liu, C.-Y. Yue and X.-W. Lei, *J. Mater. Chem. C*, 2021, **9**, 9952-9961.
9. Q. Ren, J. Zhang, Y. Mao, M. S. Molokeev, G. Zhou and X. M. Zhang, *Nanomaterials*, 2022, **12**.
10. J.-Y. Li, C.-F. Wang, H. Wu, L. Liu, Q.-L. Xu, S.-Y. Ye, L. Tong, X. Chen, Q. Gao, Y.-L. Hou, F.-M. Wang, J. Tang, L.-Z. Chen and Y. Zhang, *Adv. Funct. Mater.*, 2021, **31**, 2102848.
11. Y.-Y. Luo, Z.-X. Zhang, C.-Y. Su, W.-Y. Zhang, P.-P. Shi, Q. Ye and D.-W. Fu, *J. Mater. Chem. C*, 2020, **8**, 7089-7095.
12. L. Xu, J.-X. Gao, X.-G. Chen, X.-N. Hua and W.-Q. Liao, *Dalton Trans.*, 2018, **47**, 16995-17003.
13. C. Jiang, N. Zhong, C. Luo, H. Lin, Y. Zhang, H. Peng and C.-G. Duan, *ChemComm.*, 2017, **53**, 5954-5957.
14. M.-H. Jung, *Dalton Trans.*, 2023, **52**, 3855-3868.
15. H. Peng, B. Zou, Y. Guo, Y. Xiao, R. Zhi, X. Fan, M. Zou and J. Wang, *J. Mater. Chem. C*, 2020, **8**, 6488-6495.
16. W. Mao, J. Wang, X. Hu, B. Zhou, G. Zheng, S. Mo, S. Li, F. Long and Z. Zou, *J. Saudi Chem. Soc.*, 2020, **24**, 52-60.
17. M. Li, J. Zhou, M. S. Molokeev, X. Jiang, Z. Lin, J. Zhao and Z. Xia, *Inorg.Chem.*, 2019, **58**, 13464-13470.
18. Y. Guo, J. Wu, W. Liu and S.-P. Guo, *Inorg. Chem.*, 2022, **61**, 11514-11518.
19. J.-B. Luo, J.-H. Wei, Z.-Z. Zhang, Z.-L. He and D.-B. Kuang, *ngew. Chem.*, 2023, **62**, e202216504.
20. T. Jiang, W. Ma, H. Zhang, Y. Tian, G. Lin, W. Xiao, X. yu, J. Qiu, X. Xu, Y. Yang and D. Ju, *Adv. Funct. Mater.*, 2021, **31**.
21. G. Zhou, Z. Liu, M. S. Molokeev, Z. Xiao, Z. Xia and X.-M. Zhang, *J. Mater. Chem. C*, 2021, **9**, 2047-2053.